Complexity measures of geomagnetic indices in the last two solar cycles

T. Alberti[a,*], G. Consolini[a] and P. De Michelis[b]

[a]INAF-Istituto di Astro isica e Planetologia Spaziali, via del Fosso del Cavaliere 100, 00133 Roma, Italy
[b]Istituto Nazionale di Geo isica e Vulcanologia, via di Vigna Murata 605, 00143 Roma, Italy

ARTICLE INFO

Keywords:
Near-Earth electromagnetic environment dynamics
Geomagnetic indices
Hilbert-Huang Transform (HHT)
Complexity measures
Space Weather

ABSTRACT

The SYM-H and AE geomagnetic indices can be considered as proxies of the response of the Earth's magnetosphere and ionosphere to solar magnetic activity. They indirectly monitor some electric current systems which flow in the ionosphere and magnetosphere whose dynamics are directly or indirectly related to the Sun-Earth interaction. Consequently, their temporal changes reflect processes occurring in the near-Earth space, which contribute differently to the over-all magnetosphere-ionosphere dynamics. The aim of this work is to characterize the nature of these two geomagnetic indices by following a complex system approach and applying a novel formalism, e.g., the EMD-based dominant amplitude multifractal formalism (EMD-DAMF). A

set of complexity measures, i.e., the Hurst exponent ($\mathcal{H}$), the singularity width ($\Delta\alpha$) and the spectrum width (Δf), is evaluated for both geomagnetic indices analyzing data recorded during the last two solar cycles. One of the most significant findings of this study is the absence of relevant differences between the two solar cycles in terms of complexity measures for both geo-magnetic indices, suggesting that only the occurrence and the frequency of geomagnetic storms and substorms affect the Hurst exponent and the singularity widths of SYM-H and AE indices. Moreover, while the AE index complexity measures do not show a significant dependence on geomagnetic activity, the SYM-H index shows a reduction in its complexity features during the geomagnetic storms, manifesting a more persistent behavior and moving from a (mono)fractal-like to a multifractal-like behavior when passing from quiet to disturbed periods. Finally, our findings are consistent with previous works on the forecast horizon of the geomagnetic activity as well as on the relation between the high-latitude ionosphere and the low-latitude magneto-sphere, thus confirming the importance of providing higher resolution measures for correctly dealing with several Space Weather phenomena.

1. Introduction

The near-Earth electromagnetic environment, comprising the magnetosphere and the ionosphere, belongs to the class of the complex systems, i.e., to those systems which are characterized by a large number of interacting parties and whose global behavior cannot be considered as the sum of the activities of singular parties (Ott, 2002). This system commonly exhibits features such as for example hierarchical self-organization, scale-invariance, and criticality over a wide range of time scales (Klimas, Vassiliadis, Baker and Roberts, 1996; Consolini and Chang, 2001; Uritsky, Klimas and Vassiliadis, 2002; Chang, Tam, Wu and Consolini, 2003; Vassiliadis, 2006). Its dynamics is mainly controlled by the solar wind, which is also responsible of the shape and the size of the magnetosphere, and by processes which mainly occur inside the system and are associated with the several electric current systems flowing in the magnetosphere and ionosphere at different latitudes (e.g., Kamide, 1990; Gonzalez, Joselyn, Kamide, Kroehl, Rostoker, Tsurutani and Vasyliunas, 1994; Lyon, 2000; Borovsky and Osmane, 2019). The effects produced by these electric currents on the magnetic field can be monitored by using different geomagnetic indices derived from the time variations of the magnetic field recorded at geomagnetic observatories at high and low latitudes (Davis and Sugiura, 1966; Iyemori, 1990). These indices can be consequently considered as proxies of those electric currents which are the main sources of the recorded magnetic field variations. For example, high-latitude magnetic observations are used to derive the auroral electrojet indices (AE, AL, AU, AO), which provide a quantitative measure of the level of magnetic activity in the auroral zone due to the high-latitude ionospheric currents flowing below and within the auroral oval, e.g., the auroral

*Corresponding author
tommaso.alberti@inaf.it (T. Alberti); giuseppe.consolini@inaf.it (G. Consolini); paola.demichelis@ingv.it (P. De Michelis)
ORCID(s): 0000-0001-6096-0220 (T. Alberti); 0000-0002-3403-647X (G. Consolini); 0000-0002-2708-0739 (P. De Michelis)

electrojets (Davis and Sugiura, 1966). More specifically, the AL and the AU indices allow to monitor the intensity of the westward and eastward auroral electrojets, respectively, the AE index represents, in first approximation, the global activity of the two electrojets providing a measure of the overall energy deposition rate (Ahn, Akasofu and Kamide, 1983), and the AO index provides a measure of the equivalent zonal current (Ahn et al., 1983).

Over the past years, the analysis and the detailed study of these indices allowed us to derive interesting information on some processes occurring at high latitude and mainly due to the dynamical interaction between the Sun and Earth environment. For instance, it has been possible to study the morphology of substorms from both a quantitative and a qualitative point of view (Daglis, Livi, Sarris and Wilken, 1994; Uritsky and Pudovkin, 1998) and to characterize the coupling between the interplanetary medium variability and the high-latitude ionosphere (Tsurutani, Sugiura, Iyemori, Goldstein, Gonzalez, Akasofu and Smith, 1990). The low-latitude ground-based magnetic measurements are instead used to measure the magnitude of magnetic disturbance recorded on the ground in the horizontal magnetic field mainly due to the equatorial ring current, a current flowing westward in the magnetospheric equatorial plane at a distance between $3R_E$ to 8 R_E. The ground effect produced by the storm-time enhancement of this current is an intensity reduction of the geomagnetic field horizontal component. Its variations at middle and low latitudes are used to derive the SYM-H index (Iyemori, 1990). Indeed, SYM-H is computed from a network of 6 magnetic observatories evenly distributed in longitude across the equatorial region and describes the geomagnetic disturbances at low and mid latitudes in terms of longitudinally symmetric (SYM) disturbances of the horizontal (H) component of the geomagnetic field (Iyemori, 1990). Thus, this index is particularly helpful for investigating the large-scale behavior of the ring current, the dynamics and topology of geomagnetic storms and their relation with solar source phenomena (Wanliss, 2005; Wanliss and Uritsky, 2010).

A common feature of AE and SYM-H time series is their irregular and bursty nature which reflects the intrinsic chaotic/complex nature of the near-Earth electromagnetic environment that they indirectly describe (Sharma, 1995; Consolini, 2002; Consolini, Alberti and De Michelis, 2018). What we know about the complexity features of these indices is largely based on different approaches applied in the years: the canonical structure function analysis (Takalo, Lohikoski and Timonen, 1995; Borovsky and Valdivia, 2018), the multifractal detrended fluctuation analysis (Wanliss, 2005), and so on (Consolini, Marcucci and Candidi, 1996). For example, these previous studies have established, that the variability of AE-index is characterized by a hierarchy of scaling exponents, that reflect the intermittent and multifractal nature of high-latitude magnetic fluctuations (Consolini et al., 1996), and that its fluctuations have a non-Gaussian character (Consolini and De Michelis, 1998), which suggests the lack of a global self-similarity property. An implication of this is the possibility that, although the solar wind variability greatly influence the AE index, especially on large timescales (Consolini and De Michelis, 2005; Alberti, Consolini, Lepreti, Laurenza, Vecchio and Carbone, 2017a), the intermittent character of the AE index and of solar wind parameters can have a different origin. Indeed, it has been found that the solar wind fluctuations within the inertial regime follow a Kolmogorov-like behavior $f^{-5/3}$ that is the result of a nonlinear cascade process (Bruno and Carbone, 2016) conversely, the AE index fluctuations follow a f^{-2} behavior probably due to a stochastic cascade/multiplicative avalanching process (Consolini, 2002). This behavior is a peculiar feature of short-term AE index fluctuations and is mainly associated with the burst activities of the magnetosphere and with the phenomenon of the release in the high-latitude ionosphere of energy stored in the magnetotail during the magnetic substorms.

Conversely, previous analysis on the complexity features of the SYM-H index suggested a stronger link with the solar wind parameters than that found in the case of the AE index. Indeed, the complexity features of the SYM-H index reveal a different character during geomagnetically quiet and disturbed periods thus suggesting a different fractal nature of the SYM-H index as a function of the geomagnetic activity levels. It has been suggested by Wanliss (2005) that the SYM-H complexity features are on average well-described by a fractional Brownian motion (fBm). However, the large, intermittent and irregular fluctuations, related to both the solar wind forcing and to the internal magnetospheric dynamics (Wanliss and Uritsky, 2010), could in principle modify the scaling properties, thus requiring a proper investigation of several possible scenarios. As an example, while during the geomagnetically quiet periods the fluctuations of the SYM-H index are characterized by an anti-persistent behavior with values of the Hurst exponent less than 0.5 ($\mathcal{H} \leq 0.5$), during the disturbed periods the values of this exponent tend to increase suggesting the tendency of the fluctuations to cluster along a direction. This means that a more ordered dynamics is observed during disturbed periods,and this may be a consequence of the large scale convection enhancement (Balasis, Daglis, Kapiris, Mandea, Vassiliadis and Eftaxias, 2006; Balasis, Daglis, Papadimitriou, Kalimeri, Anastasiadis and Eftaxias, 2009).

These findings suggest that the two geomagnetic indices, which indirectly describe different electric current systems flowing in the ionosphere and magnetosphere, are characterized by a different degree of complexity that must be taken

into account in their forecast horizon through predictive tools (Consolini et al., 2018).

Here, we focus on the investigation of complexity measures of the SYM-H and AE indices during the last two solar cycles (e.g., SC23 and SC24) introducing a novel formalism, which is based on the characterization of multiscale fluctuations and statistical properties for non-stationary and nonlinear time series. One of the most significant findings from our study is that the strength of the solar activity cycle does not significantly affect the complexity measures of both geomagnetic indices. They seem to be mainly affected by the occurrence and frequency of solar perturbations. Furthermore, the complexity measures of the AE index do not show a clear degree of correlation with the geomagnetic activity. Conversely, the complexity measures of the SYM-H index significantly change passing from a quiet to a disturbed period. Indeed, all complexity measures related to the SYM-H index (e.g., the Hurst exponent and the multifractal widths) show a clear degree of correlation with the geomagnetic activity and suggest a weakly multifractal nature, which is always present regardless by the magnetic activity level. Finally, our findings also support the existence of a relation between the processes that take place in the high-latitude ionosphere and those that occur in the low-latitude magnetosphere.

2. Data

In this study we have considered data from the last two solar cycles, i.e., solar cycle 23 and 24 (SC23, SC24), spanning the period of time between January 1997 to January 2018. Although the end time of solar cycle 24 is the late 2019, due to the temporal availability of the AE index we have restricted the time interval to January 2018 (`https://cdaweb.gsfc.nasa.gov/index.html/`). For this time interval we have considered three different quantities: the daily total sunspot number, the SYM-H index and the AE index. The daily total sunspot number (SSN) has been freely retrieved from WDC-SILSO[1] and has been derived by the formula $\mathrm{SSN} = N_s + 10N_g$, with N_s and N_g the number of spots and groups counted over the entire solar disk, respectively (Clette, Svalgaard, Vaquero and Cliver, 2014). The SYM-H and AE geomagnetic indices time series, with one-minute resolution, are obtained from the CDAWeb interface at `https://cdaweb.gsfc.nasa.gov/index.html/`.

Fig. 1 reports the daily total sunspot number (SSN) and the two geomagnetic indices, AE and SYM-H, during the analysed time interval. The daily total sunspot number time series clearly follows the ∼11-yr solar magnetic activity cycle. It is characterized by higher values during the solar maxima periods, e.g., 2000-2001 for SC23 and 2014 for SC24 (Laurenza, Alberti, Marcucci, Consolini, Jacquey, Molendi, Macculi and Lotti, 2019) and by lower values during the minimum phase of SC23, i.e., 2008-2009.

The temporal trend of SSN clearly shows how the solar cycle 24 has been less active than the solar cycle 23 having reached a maximum value for the SSN of ∼200 with respect to the value of ∼350 reached for the SC23 (Hathaway, 2015). The activity is not the only difference between the two solar cycles, it has been shown that energetic events such as solar energetic particle (SEP) events and ground level enhancements (GLEs) have been significantly reduced or lacked during the SC24 (Vainio, Raukunen, Tylka, Dietrich and Afanasiev, 2017). Furthermore, while the total CME rate has been very similar in the ascending and maximum phases of the two cycles, CMEs related to the SEP events in the SC24 have been faster and more expansive, implying that the coronal conditions in the two cycles have been markedly different (Gopalswamy, Akiyama, Yashiro, Xie, Mäkelä and Michalek, 2014). These results have been also confirmed by Alberti, Laurenza, Cliver, Storini, Consolini and Lepreti (2017b) in terms of a lower occurrence rate and intensity of energetic events in the SC24, as well as, in the number of intensive flares (>M5 class) (Subramanian and Shanmugaraju, 2016). These decreases can be attributed to several factors, such as a weak interplanetary magnetic field which decreases the efficiency of the particle acceleration mechanisms (Gopalswamy, Mäkelä, Yashiro, Xie, Akiyama and Thakur, 2015; Laurenza, Alberti and Cliver, 2018; Alberti, Laurenza and Cliver, 2019c).

Naturally, the low level of solar activity is also reflected on a low level of geomagnetic activity recorded on the ground. In confirmation of this, the SC24 has been characterized by a nearly 40% reduction in the number of geomagnetic storms and magnetic substorms (Selvakumaran, Veenadhari, Akiyama, Pandya, Gopalswamy, Yashiro, Kumar, Mäkelä and Xie, 2016) as it can also be revealed by the temporal trend of the two geomagnetic indices during the two different solar cycles. At least 13 intense geomagnetic storms, characterized by SYM-H<250 nT and by values of the global geomagnetic activity index (Kp) greater than 9, occurred during the SC23, as for example the well-known Bastille's Day geomagnetic storm and the Halloween superstorm (Chi, Russell, Foster, Moldwin, Engebretson and Mann, 2005; Tsurutani, Judge, Guarnieri, Gangopadhyay, Jones, Nuttall, Zambon, Didkovsky, Mannucci, Iijima,

[1] `http://sidc.be/silso/home`

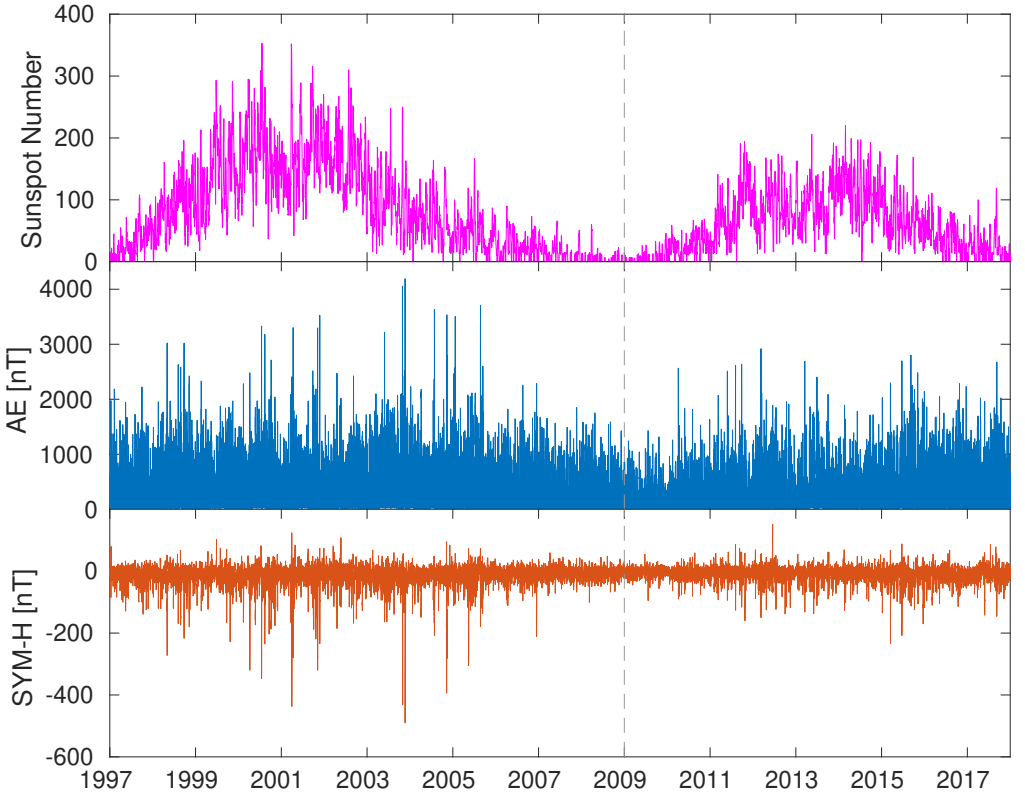

Figure 1: From the top to bottom: The daily total sunspot number (magenta), the AE index (blue), and the SYM-H index (orange) across solar cycles 23 and 24. The gray dashed line marks the transition from the solar cycle 23 to the solar cycle 24.

Meier, Immel, Woods, Prasad, Floyd, Huba, Solomon, Straus and Viereck, 2005; Balasis, Daglis, Zesta, Papadimitriou, Georgiou, Haagmans and Tsinganos, 2012). Conversely, there have been no geomagnetic storms with the same strength during the SC24. During this solar cycle the strongest geomagnetic storm is that occurred on 17 March 2015, known as St. Patrick's Day storm, during which the value of the global geomagnetic activity index has been equal to $Kp = 8$ (Kamide and Kusano, 2015; Wu, Liou, Lepping, Hutting, Plunkett, Howard and Socker, 2016; Carlyle, van Driel-Gesztelyi, Zuccarello, James and Williams, 2017).

3. Methods

3.1. Empirical Mode Decomposition (EMD)

The Empirical Mode Decomposition (EMD) is a decomposition method proposed to overcome some limitations of previous time series analysis as the linearity and/or stationarity requirements (Huang, Shen, Long, Wu, Shih, Zheng, Yen, Tung and Liu, 1998). Indeed, by means of the sifting process, whose main steps are reported in Table 1, any a priori mathematical assumption is removed, because the process completely empirical and based on the local properties of the time series (Huang et al., 1998; Huang and Wu, 2008). From a numerical point view, several stopping criteria have been proposed to suitably stop the sifting process, avoiding an infinite number of steps (Huang et al., 1998; Huang and Wu, 2008; Alberti et al., 2017a; Alberti, Lekscha, Consolini, De Michelis and Donner, 2020). The most used criterion is that based on the difference between two successive iterations as measured in terms of the standard deviation (Huang et al., 1998), although several refinements have been made to take into account not only global excursions but also local variations (Flandrin, Rilling and Goncalves, 2004). According to this adaptive data analysis

Table 1
The main steps of the sifting process.

$\mathcal{X}(t) \rightarrow \mathcal{X}_m(t) = \mathcal{X}(t) - \langle \mathcal{X}(t) \rangle$ $\delta(t) = \mathcal{X}_m(t)$
1. find local extrema of $\delta(t)$ 2. find upper and lower envelopes by using cubic spline $\rightarrow \mathcal{U}(t)$, $\mathcal{L}(t)$ 3. find the mean envelope $\rightarrow \mathcal{M}(t) = \frac{\mathcal{U}(t)+\mathcal{L}(t)}{2}$ 4. update $\delta(t) \rightarrow \delta(t) - \mathcal{M}(t)$
if $\delta(t)$ is an IMF store $C_j(t) = \delta(t)$ $\delta(t) \rightarrow \delta(t) = \mathcal{X}_m(t) - \delta(t)$ repeat steps 1.-4. **else** iterate steps 1.-4. until $\delta(t)$ is an IMF store $C_j(t) = \delta(t)$ $\delta(t) \rightarrow \delta(t) = \mathcal{X}_m(t) - \delta(t)$ repeat steps 1.-4.
stop the process when $\rho(t) = \delta(t)$ is a non-oscillating function or has only two extrema

method any time-dependent signal $\mathcal{X}(t)$ can be written in the following form:

$$\mathcal{X}(t) = \sum_{j=1}^{N} C_j(t) + \mathcal{R}(t) \tag{1}$$

where the set $\{C_j(t)\}$, named as Intrinsic Mode Functions (IMFs) or empirical modes, is the decomposition basis, while $\mathcal{R}(t)$ is the residue of the decomposition. According to Huang et al. (1998) an IMF is defined as a function having the same (or differing at most by one) number of extrema and zero crossings and a zero-average mean envelope derived from local maxima and minima envelopes. Furthermore, the decomposition basis $\{C_j(t)\}$ a posteriori satisfies mathematical requirements of completeness, convergence, and local orthogonality (Huang et al., 1998).

3.2. Hilbert Spectral Analysis (HSA)

The EMD is the first and fundamental step for correctly applying the Hilbert Transform (HT), which allows us to have information on the energy-time-frequency distribution in a time series (e.g., Huang et al., 1998). Indeed, given an empirical mode $C_j(t)$ we can define its Hilbert Transform $\hat{C}_j(t)$ as

$$\hat{C}_j(t) = \frac{1}{\pi} \mathcal{P} \int_0^T \frac{C_j(t')}{t - t'} dt' \tag{2}$$

where $\mathcal{P}$ the Cauchy principal value and T the length of time series. By introducing the complex signal

$$\mathcal{Z}_j(t) = C_j(t) + i\, \hat{C}_j(t) = \mathcal{A}_j(t)\, exp \left\{ i\, 2\pi \int_0^T \omega_j(t') dt' \right\} \tag{3}$$

the new concepts of instantaneous amplitude $\mathcal{A}_j(t)$ and instantaneous frequency $\omega_j(t)$ immediately come out as

$$\mathcal{A}_j(t) = \sqrt{C_j^2(t) + \hat{C}_j^2(t)}, \tag{4}$$

$$\omega_j(t) = \frac{d}{dt} \tan^{-1} \left[\frac{\hat{C}_j(t)}{C_j(t)} \right]. \tag{5}$$

Thus, for each empirical mode a mean timescale of oscillation, giving us information on the characteristic scale of the observed fluctuations, can be derived as

$$\tau_j = \langle \omega_j^{-1}(t) \rangle_t, \tag{6}$$

with $\langle \dots \rangle_t$ identifying the time average.

Taking into account the time dependency of both amplitudes and frequencies of the empirical modes, Huang et al. (1998) introduced a three-dimensional representation of the energy-time-frequency distribution of a signal by contouring the squared values of amplitudes on a time-frequency plane. This representation is the so-called Hilbert-Huang spectrum $h(t', \omega')$, with $t' \in [0, T]$ and $\omega' \in [\min\{\omega_j(t)\}, \max\{\omega_j(t)\}]$. The global information over frequencies can be investigated by integrating over time the Hilbert-Huang spectrum, thus recovering the so-called Hilbert marginal spectrum

$$h(\omega') = \int_0^T h(t', \omega') dt', \tag{7}$$

although global information can be also simply derived by looking at the behavior of the variance of each empirical mode with respect to the mean timescales, thus providing a fast and quick-look approach for identifying the different dynamical regimes. Finally, an intermittency measure can be introduced as

$$DS(\omega') = \frac{1}{T} \int_0^T \left[1 - \frac{h(t', \omega')}{h(\omega)} \right]^2 dt', \tag{8}$$

also called Degree of Stationarity (DS), being a time series statistically stationary if DS ≤ 1 (Huang et al., 1998). This is of primary interest when some complexity measures and fractal approaches are investigated (Alberti, Consolini, Carbone, Yordanova, Marcucci and De Michelis, 2019b).

3.3. The EMD-based multifractal analysis (EMD-DAMF)

In 2013 Welter and Esquef (2013) proposed an EMD-based method for detecting complexity measures by partitioning the time and scale domain of a signal into fractal dimension regions. It allows to investigate singularities and fractal measures of time series by means of the following steps:

1. apply the EMD and HSA methods for deriving instantaneous amplitudes $\mathcal{A}_j(t)$ and mean timescale τ_j;
2. by defining a support $\mathcal{I}_{j,\ell}$ around the $\ell-$th local maximum determine the dominant amplitude coefficients $\mathcal{D}_{j,\ell}$

$$\mathcal{D}_{j,\ell} \doteq \sup_{j' \leq j} \left\{ \max \left\{ |\mathcal{A}_{j'}(t \in I_{j,\ell})| \right\} \right\} \tag{9}$$

   with $\ell = 1, \dots, N_j$, being N_j the number of local maxima of $\mathcal{A}_j(t)$;
3. define the $q-$th–order structure function $S_q(\tau)$

$$S_q(\tau) = \frac{1}{N_j} \sum_{j=1}^{N_j} \mathcal{D}_{j,\ell}^q; \tag{10}$$

4. evaluate the scaling exponent $\zeta(q)$

$$\zeta(q) = \frac{\log S_q(\tau)}{\log \tau}; \tag{11}$$

5. estimate the singularity strengths α and spectrum $f(\alpha)$ by means of a Legendre transform of $\zeta(q)$

$$\alpha = \frac{d\zeta(q)}{dq} \tag{12}$$

$$f(\alpha) = \alpha q - \zeta(q). \tag{13}$$

This procedure allows to derive the scaling features of time series by exploiting the local features of empirical modes, i.e., based on the local extrema, thus allowing a more proper evaluation of differences/increments between two points with respect to the usual structure function analysis. Furthermore, the structure functions are evaluated at different timescales, which are the characteristic timescales of the empirical mode, instead of fixing them a priori. This also allows to deal with a small number of points over which the scaling exponents are evaluated. As for canonical

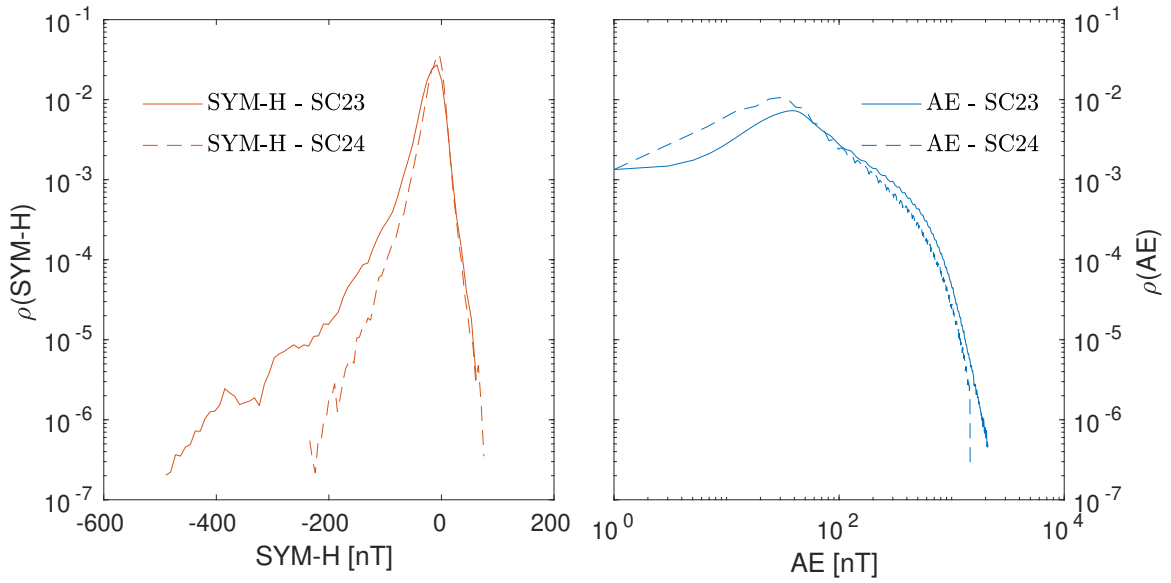

Figure 2: Probability distribution functions of the SYM-H index (orange) and the AE index (blue), respectively. Continuous and dotted lines refer to the solar cycle 23 and 24, respectively.

structure function analysis, we can identify some crucial and interesting complexity measures as the Hurst exponent $\mathcal{H}$, the singularity width $\Delta\alpha = \alpha_{\max} - \alpha_{\min}$, and the singularity spectrum width $\Delta f = f_{\max} - f_{\min}$, allowing us in characterizing the complex fractal nature of time series (Ott, 2002).

The Hurst exponent measures the long-term memory of time series, characterizing its persistent nature (Harold, 1951). Indeed, if $\mathcal{H} \in [0, 0.5)$ then the time series values switch between high and low values in adjacent pairs, if $\mathcal{H} \in (0.5, 1]$ then the time series has a long-term positive autocorrelation, while if $\mathcal{H} = 0.5$ then the time series has a completely uncorrelated behavior (Harold, 1951; Mandelbrot, 1982). The singularity measures, e.g., the singularity width $\Delta\alpha$ and the singularity spectrum width Δf, are used to characterize the range of singularities and the range of Hausdorff dimensions that are present in a time series, quantifying the multifractal nature of a time series (Hausdorff, 1918; Mandelbrot, 1982; Ott, 2002).

4. Results and discussions

We start our analysis by evaluating the probability distribution functions (PDFs) ρ of the two selected geomagnetic indices, SYM-H and AE, during the solar cycles SC23 and SC24. We identified the boundaries of both solar cycles as proposed in Tsurutani, Echer and Gonzalez (2011) who showed that minima in the SC22 and SC23 occurred later than sunspot number minima by a half of year. Thus, in the following we identifythe SC23 and SC24 periods as the time intervals between mid-1997–mid-2009 and mid-2009–2018. Fig. 2 reports the results obtained from the analysis of the SYM-H index (left panel) and of the AE index (rigth panel), respectively. What is interesting about the data in this figure is that differences can be observed comparing the PDFs of the two indices evaluated during the two different solar cycles. In the case of the SYM-H index, the PDF evaluated during the SC23 is significantly different from what is obtained during the SC24. The left side tail of the PDF, which is associated with more negative SYM-H values, is higher in the SC23 than in the SC24. This is essentially due to a larger number of strong geomagnetic storms occurred during SC23 (Selvakumaran et al., 2016) than SC24. The PDFs of the AE index are also different in the two solar cycles although this difference is less notable. It is mainly concentrated in correspondence of the lower AE values. During the SC24 the periods characterized by a low/very-low/quiet geomagnetic activity, and consequently by low values of the AE index, have been in greater numbers than those in SC23. That is reflected in higher values of the AE PDF at lower AE values during the SC24 than SC23. These findings seem to suggest that both indices depend on the strength of the solar activity, although the SYM-H index seems to be more affected than the AE index. The different behaviour of the two indices can be due to the different processes and current systems affecting them, which depend

differently on the interplanetary magnetic field conditions. Indeed, the AE index is more sensitive to both the directly-driven processes, occurring on long timescales and mainly due to magnetospheric convection driven by long-standing reconnection phenomena at the Earth's magnetopause, and the magnetotail dynamics, related to fast energy releases (loading-unloading phenomena). The latter component of the AE index manifests in coherent intermittent activity bursts whose typical timescales are shorter than 200 min (90-100 min) (Kamide and Kokubun, 1996; Consolini and De Michelis, 2005). Because the former process (the loading-unloading) essentially dominates on the variability range of the AE-index, this index is mainly dependent on the dynamical processes taking place inside the magnetosphere occurring in the magnetotail (Consolini and De Michelis, 2005), thus explaining the less sensitivity to the strength of solar activity with respect to the SYM-H index.

Conversely, in the SYM-H index a fundamental role is played by the large plasma convection processes, which occur during the geomagnetic storms generated by a long-standing reconnection process at the magnetopause, i.e., when there is a strong flow of energy, mass and momentum from the solar wind into the magnetospheric environment surrounding Earth. The conditions that are effective for creating geomagnetic storms strongly depend on the conditions of the interplanetary magnetic field orientation, which should be generally Southward oriented for a very long time. This condition is more probable during periods of high solar activity, when large mass ejected from the solar corona propagate in the interplanetary space and hit the Earth's magnetosphere. Indeed, these large-scale structures can have favorable magnetic field conditions, which last for a sufficient time to enhance the overall magnetospheric convection, leading to an enhancement of the equatorial ring current on which the SYM-H index depends. This situation is clearly more probable during periods of high than quiet solar activity level.

To better outline the different nature of the geomagnetic indices at the different timescales, for each IMF we compute the corresponding average characteristic timescale and its variance. These two quantities allow us to construct a variance-timescale distribution of empirical modes (see Fig. 3), which can be the first point to investigate the existence of different processes/phenomena. To obtain these distributions, the original time series of the two indices have been decomposed using the EMD method and successively the average energy (in terms of variance) and the mean timescale of each IMF have been evaluated according to Eq. (6). The obtained results, taking care to separate the two solar cycles, are reported in Fig. 3. The EMD allows us to derive 34 IMFs for the AE index during both solar cycles, while 34 and 32 empirical modes have been extracted for the SYM-H index during the SC23 and SC24, respectively. The variance shows a clear dependence on the timescales suggesting the existence of different classes of dynamical processes Alberti, Consolini, De Michelis, Laurenza and Marcucci (2018).

At large timescales ($\tau > 10^4$ min), we observe a small discrepancy in terms of variance between the two solar cycles in the case of SYM-H index. This is due to the SYM-H values, which are lower during SC23 than SC24, and that is reflected in a greater variance of the signal during the SC23. These large timescales are related to the characteristic timescales of solar rotational phenomena associated with magnetic structures such as high-speed streams, coronal holes, and magnetic clouds which are typically recovered into geomagnetic indices variability (Verbanac, Vršnak, Živković, Hojsak, Veronig and Temmer, 2011; Richardson and Cane, 2012). In the case of AE index at smaller timescales, a break in the scaling behavior of the variance is found at ∼200 min. This break, which is present in both solar cycles, is consistent with the nonlinear response of the AE index to the changes of interplanetary medium conditions (Tsurutani et al., 1990). Conversely, this break is not observed in the variance-timescale distribution of the SYM-H index.

Finally, the results of this investigation on the SYM-H and AE variance-timescale distributions during the two different solar cycles show that these distributions are affected by solar activity mainly at larger timescales. At mid and small timescales, there is no great difference between the trends obtained from each solar cycle. In other words, the dependence of the dynamical features of the two geomagnetic indices on solar activity seems to be confined to longer timescales, which are more directly related to the long-term variation of the solar activity.

In order to better investigate the statistical features of the two geomagnetic indices in the two selected solar cycles we have evaluated the degree of stationarity associated with each IMF obtained by decomposing the original signals according to Eq. (8). The results are reported in Fig. 4 where the trends of the degree of stationarity as a function of the timescale τ evaluated for both indices during the two different solar cycles are shown. The results suggest that a different degree of stationarity characterizes the multiscale fluctuations of the SYM-H and AE indices. While there are not significant differences in the values of the degree of stationarity of the two indices at short timescales that is around 1, a clear difference emerges at timescales longer than $\tau \sim 10^3$ min. This result suggests that the fluctuations of the two indices are statistically (non-)stationary for timescales (larger)shorter than $\tau \sim 10^3$.

The evaluation of the stationarity of the time series is a crucial point for correctly evaluating complexity measures

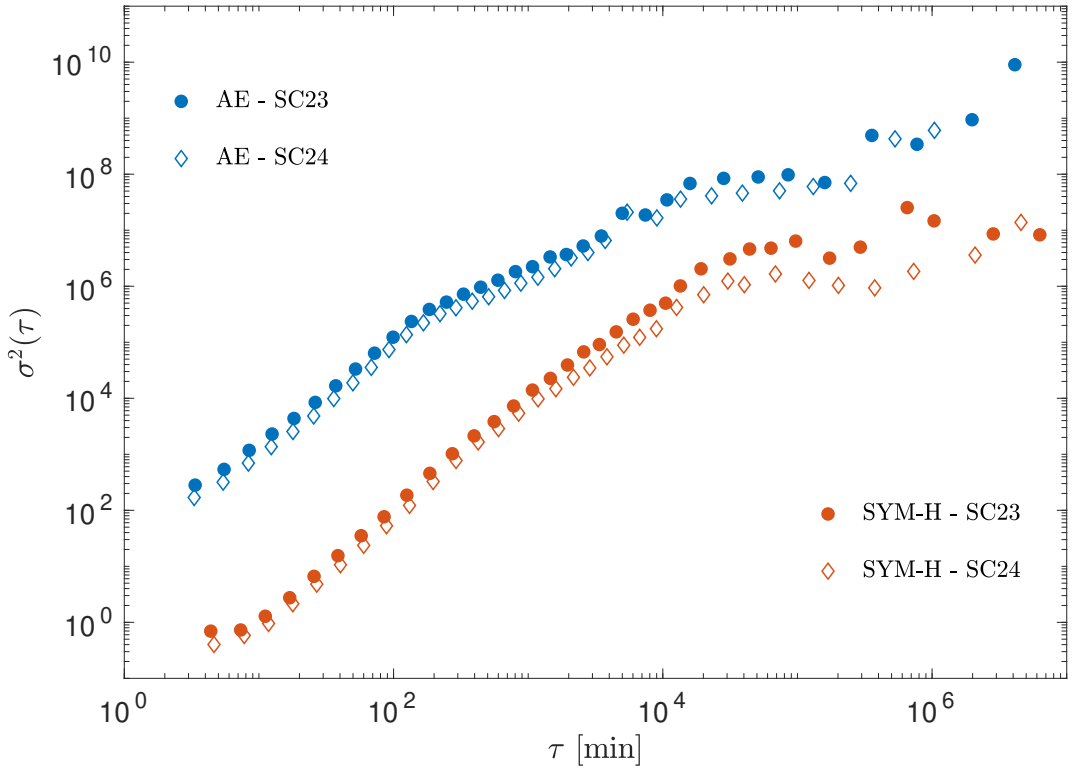

Figure 3: The variance-timescale ($\sigma^2 - \tau$) distribution of the empirical modes extracted from the AE index (blue) and the SYM-H index (orange), respectively. Circles and diamonds refer to the solar cycle 23 and 24, respectively.

as for example the Hurst exponent ($\mathcal{H}$) and the singularity features of time series (α, $f(\alpha)$, $\Delta\alpha$, Δf). Indeed, to evaluate these complexity measures is necessary that time series are stationary or non-stationary but characterized by stationary increments (Harold, 1951; Mandelbrot, 1982). Thus, the evaluation of the degree of stationarity permits us to select the range of timescales over which the time series are statistically stationary. Taking into account the results reported in Fig. 4 we can fix the range of timescales between 3 and 300 min and apply the EMD-DAMF method to compute the scaling exponents and the other complexity measures only to those IMFs satisfying the condition to have a characteristic scale below 300 min. In this way, we can be sure that the stationarity condition is satisfied.

In order to investigate the complexity of both indices we use the EMD-DAMF method to evaluate the Hurst exponent ($\mathcal{H}$), the singularity width ($\Delta\alpha$) and the singularity spectrum width (Δf) over two-day sliding windows for the total time period, thus selected without any distinction of the solar cycles. By using a two-day sliding window, we are able to correctly deal with changes into the complexity measures due to the occurrence of geomagnetic storms and substorms, thus considering both quiet and disturbed periods, and to collect a sufficient number of points for statistics of increments. Fig. 5 reports the behavior of the Hurst exponent for the two geomagnetic indices as a function of the corresponding mean values of the SYM-H and AE indices for each sliding time window. The values of the Hurst exponent have been binned into (ΔSYM-H, ΔAE) = (10, 20) nT degree-sized bins. The values of the Hurst exponent associated with the AE index are on average higher than those associated with the SYM-H index.

The values of the Hurst exponent associated with the SYM-H index depend on the geomagnetic activity level. This accords with some earlier observations (e.g., Wanliss, 2005; Balasis et al., 2006; Balasis, Daglis, Papadimitriou, Kalimeri, Anastasiadis and Eftaxias, 2008; Balasis et al., 2009), which showed that the SYM-H index is characterized by high values of $\mathcal{H}$ during disturbed periods and by lower values during quiet ones. A possible explanation for this might be that there is an increase of the self-organization of the overall magnetospheric activity during geomagnetic storms which is the main responsible of the more persistent behavior of the signal. Thus, the increasing trend of $\mathcal{H}_{\text{SYM-H}}$

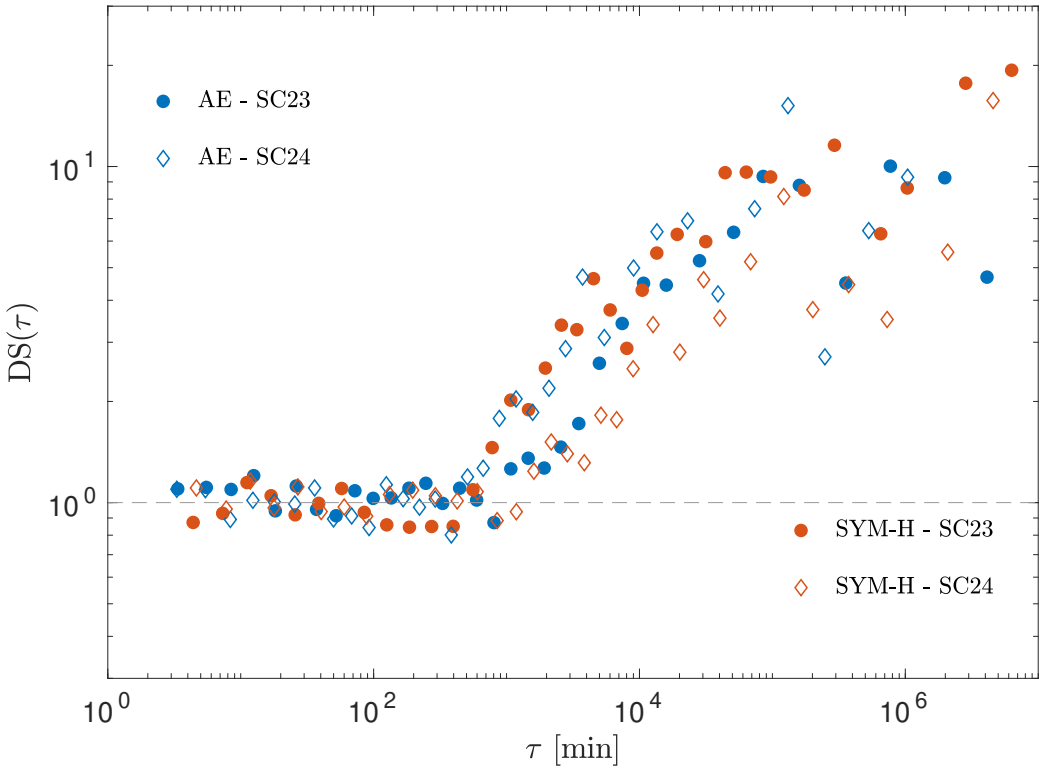

Figure 4: Degree of stationarity (DS) of the AE index (blue) and the SYM-H index (orange), respectively. Circles and diamonds refer to the solar cycle 23 and 24, respectively. The gray dashed line refers to DS(τ) =1.

values with the geomagnetic activity suggests a certain degree of correlation with the occurrence of geomagnetic storms and substorms. This dependence of the $\mathcal{H}$ values on the geomagnetic activity is not found in the case of the AE index. Indeed, the $\mathcal{H}_{\mathrm{AE}}$ does not seem to show any pattern or trend with the geomagnetic activity level, being more or less confined in the range 0.4 - 0.6. The dependence of $\mathcal{H}_{\mathrm{SYM\text{-}H}}$ on the geomagnetic activity suggests that this quantity displays a certain degree of correlation with the occurrence of geomagnetic storms and substorms, as monitored both by SYM-H and AE. A possible explanation of the dependence of $\mathcal{H}_{\mathrm{SYM\text{-}H}}$ on substorms activity (i.e., on AE-index) could be the existence of a link between high-latitude phenomena and ring current enhancement during magnetic storms (De Michelis, Consolini, Materassi and Tozzi, 2011; Stumpo, Consolini, Alberti and Quattrociocchi, 2020). The existence of such a link is also supported by in-situ observations (Daglis, Axford, Livi, Wilken, Grande and Søraas, 1996).

In order to investigate the existence of a possible link between multifractal features and the geomagnetic activity level we evaluate the singularity width $\Delta\alpha$, which provides information on range of singularities, i.e., on the degree of intermittency. Fig. 6 reports the obtained results as a function of the Hurst exponent for both solar cycles independently. No significant dependence on the solar cycle activity is found for both geomagnetic indices. This result suggests that complexity features do not significantly depend on the strength of solar cycle but only on occurrence of geomagnetic storms and substorms. Moreover, there is no evidence of a clear pattern of complexity for the AE index, being characterized by large values of the singularity width $\Delta\alpha$. That confirms the multifractal and intermittent nature of the auroral electrojet variability despite the geomagnetic activity level (Consolini et al., 1996; Consolini and De Michelis, 1998).

What is really interesting is the behavior of the complexity measures of the SYM-H index. A clear increasing pattern seems to emerge suggesting that intermittency and multifractal features appear when the Hurst exponent increases (e.g., when the geomagnetic activity level tends to increase). This supports previous findings by Wanliss (2005) and allows us to directly relate the increases in the persistency of the SYM-H index during the main and the recovery

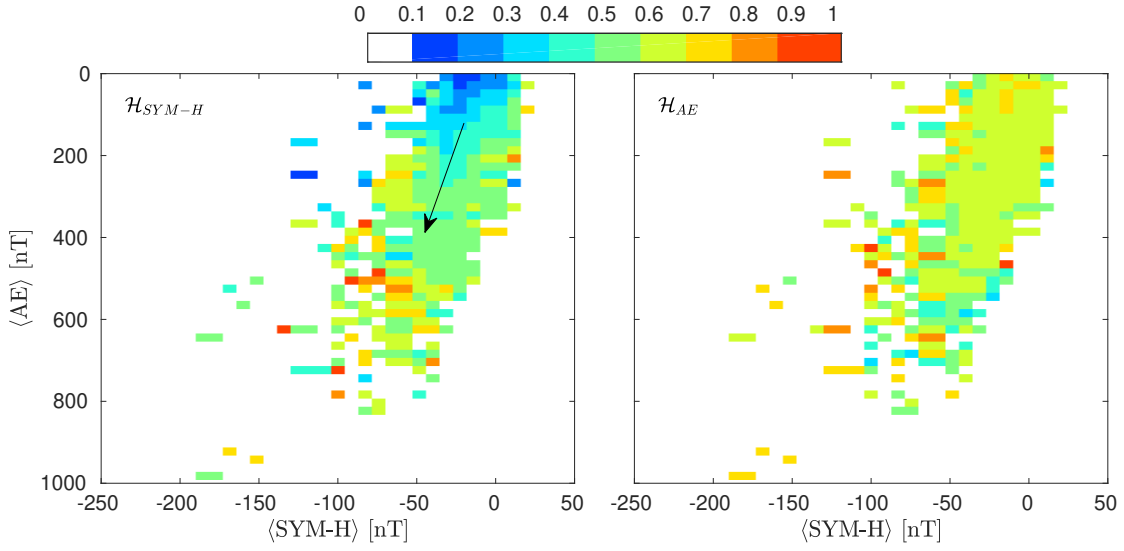

Figure 5: The Hurst exponent ($\mathcal{H}$) for SYM-H (left panel) and AE (right panel) as a function of the corresponding mean values of SYM-H and AE indices for each sliding time window. The black arrow represents the main direction of the dependence of $\mathcal{H}_{\text{SYM-H}}$ on the geomagnetic activity.

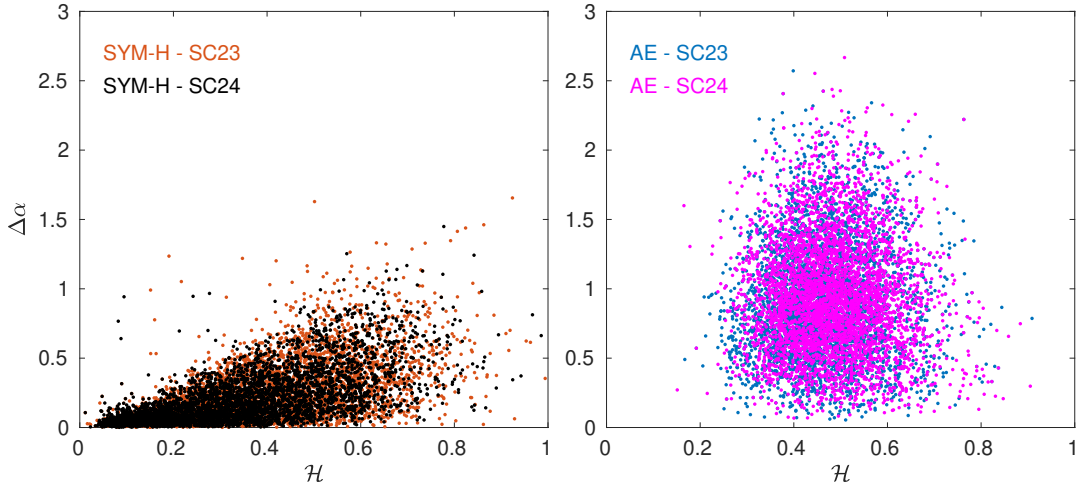

Figure 6: The singularity width $\Delta\alpha$ versus the Hurst exponent $\mathcal{H}$ for SYM-H (left panel) and AE (right panel) during the solar cycles 23 and 24, respectively.

phases of a geomagnetic storm ($\mathcal{H}_{\text{SYM-H}}$) to intermittent burst activity ($\Delta\alpha > 0.5$). This relation can be also confirmed by evaluating the mutual information coefficient (MI) between the Hurst exponent and the singularity width for both geomagnetic indices and during the two solar cycles. In the framework of information theory, the mutual information between to signals provides an overall measure of the correlation degree (both linear and nonlinear) between them. In detail, given two dataset $\{x_i, y_i\}$, indicating with $p(x)$ and $p(y)$ the corresponding probabilities of observing a specific value for x and y, the mutual information $MI_{x,y}$ is defined as

$$MI_{x,y} = \sum_{j,k} p(x_j, y_k) \ln \frac{p(x_j, y_k)}{p(x_j)p(y_k)} \tag{14}$$

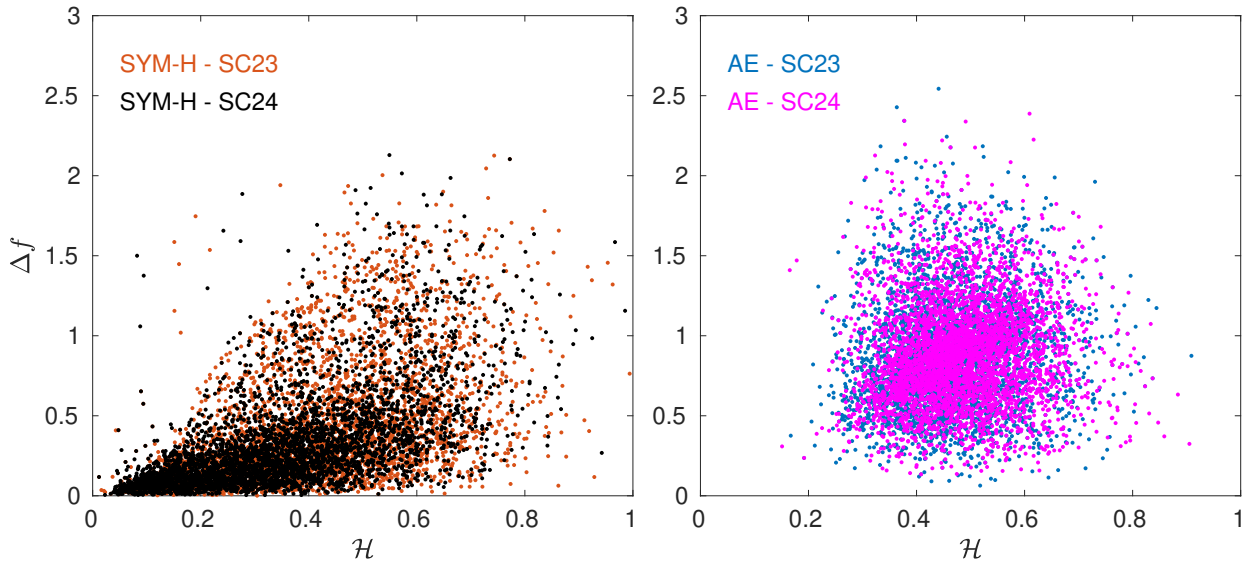

Figure 7: The singularity spectrum width Δf versus the Hurst exponent $\mathcal{H}$ for SYM-H (left panel) and AE (right panel) during the solar cycles 23 and 24, respectively.

where $p(x_j, y_k)$ is the joint probability for observing the duplet (x_j, y_k). For two independent time series $MI_{x,y} = 0$. Thus, we can use this quantity to estimate the correlation degree between the Hurst exponent ($\mathcal{H}$) and the singularity width ($\Delta\alpha$). The results obtained from the evaluation of the mutual information suggest that there is a good correlation between $\mathcal{H}_{\text{SYM-H}}$ and $\Delta\alpha_{\text{SYM-H}}$ ($MI = 0.28$ and $MI = 0.55$ for SC23 and SC24, respectively, being the 95% confidence levels $CL_{95} = 0.08$ for both solar cycles), while we do not find any evidence of a correlation in the case of the complexity measures associated with the AE index ($MI = 0.01$ and $MI = 0.02$ for SC23 and SC24, respectively, being the 95% confidence levels $CL_{95} = 0.04$ for both solar cycles).

Similar results are also obtained by investigating the behavior of the singularity spectrum width Δf as a function of the Hurst exponent during the two different solar cycles (see Fig. 7). A clear correlation is found for increasing values of the Hurst exponent and of singularity spectrum width in the case of the SYM-H index during both solar cycles. Conversely, no significant correlation is observed in the case of AE index. This suggests that during both the main and the recovery phases of a geomagnetic storm, e.g., when the SYM-H index shows a persistent behavior, there is also an increase of the Hausdorff dimensions. Since the higher the Hausdorff dimensions the lower the complexity, this means that during a geomagnetic storm we can observe a smoother (multi)fractal behavior, which suggests a reduction of chaos and a consequently tendency of the system to move towards a more predictable dynamic Alberti, Consolini and Carbone (2019a). This also accords with our earlier observations (Consolini et al., 2018), which showed that the overall magnetospheric dynamics as monitored by the SYM-H is characterized by an increase of the forecast horizon during a disturbed period. Conversely, during quiet periods, e.g., when $\mathcal{H}_{\text{SYM-H}} < 0.5$, an increased in the chaotic nature of the SYM-H index is observed, as confirmed by the reduction in the singularity spectrum width Δf, with the system becoming monofractal in its nature. Finally, the significance of the results has been also assessed with respect to the intrinsic long-tailed nature of AE and SYM-H distributions, being characterized by high kurtosis and high skewness. By using two newly defined time series, i.e., log(AE) and log(|SYM-H| + 0.5), having low kurtosis and low skewness, we found (not shown) that our findings on the behavior of the Hurst exponent, related the persistent nature of time series, as well as on the fractal measures and nature (i.e., mono vs. multifractal behavior, intermittency nature) are not affected by the shape of distributions, thus confirming our conclusions on the complexity nature of both AE and SYM-H.

5. Conclusions and perspectives

By using a novel formalism, e.g., the EMD-based dominant amplitude multifractal formalism (EMD-DAMF), this study investigates the complexity features of two different geomagnetic indices, SYM-H and AE, recorded during the last two solar cycles (SC23 and SC24). One of the more significant findings that emerges from this study is that there are not differences between the two solar cycles in terms of the complexity measures for both geomagnetic indices, suggesting that only the occurrence and frequency of geomagnetic storms and substorms affect the Hurst exponent and the singularity widths of the two geomagnetic indices, SYM-H and AE, respectively.

The research has also shown that the AE index is characterized by Hurst exponent values which fluctuate around $\mathcal{H}_{\mathrm{AE}} = 0.5$ and by a clear multifractal nature, which are the manifestation of the occurrence of intermittency in the high-latitude magnetic field fluctuations (Consolini et al., 1996). Indeed, being the AE index variability mostly related to fast relaxation processes occurring in the magnetotail as intermittent coherent bursts due to unloading process, its complexity property, as measured by the Hurst exponent,is less sensitive to the solar activity strength and the interplanetary medium variability with respect to the SYM-H index, but mainly depends on internal magnetospheric conditions and, in particular, on the magnetotail central plasma sheet (CPS) conditions.

This study has also revealed that the SYM-H index is characterized by complexity measures which change moving from quiet and disturbed periods. It shows a significant increase of $\mathcal{H}$ values during disturbed periods, when the externally driven fluctuations become larger, showing a clear intensification of the geomagnetic activity. This is consistent with the role played by solar wind fluctuations during geomagnetic storms, which provide an increase in the persistent nature of the SYM-H index during the main and the recovery phases of a geomagnetic storm as well as in their intermittent bursts activity ($\Delta\alpha > 0.5$). Moreover, the increasing values of the Hurst exponent can be directly related to the increasing values of the singularity spectrum width thus suggesting that during both the main and the recovery phases of a geomagnetic storm there is also an increase of the Hausdorff dimensions. This implies that during a geomagnetic storm a smoother multifractal behavior is observed, suggesting a reduction of chaos moving towards a more predictable dynamic. Conversely, an increase in the chaotic nature of the SYM-H index is observed during geomagnetically quiet periods.

These findings have significant implications for the understanding of how to model the geomagnetic response to the solar activity. One of the main results is that the complexity properties of geomagnetic indices does not only depend on interplanetary medium variability but also on phenomena related to the internal dynamics of the magnetosphere as fast relaxation processes, loading-unloading mechanisms, and so on (Consolini and De Michelis, 2005; Alberti et al., 2017a, 2020). The reduction in the Hausdorff dimensions observed during quiet periods is a direct consequence of the interplay between different processes taking place into different magnetospheric regions and affecting the behavior of the ring current. Furthermore, the clear dependence of the complexity measures of the SYM-H index on the geomagnetic activity suggests that there is an overall self-organization of the magnetospheric dynamics during geomagnetic storm. In particular, the evidence for a dependence of SYM-H index complexity measures also on the AE-index values supports the existence of a possible link between high-latitude processes (as monitored by AE) and ring current enhancement (as monitored by SYM-H) during geomagnetic storms (Daglis et al., 1996; De Michelis et al., 2011; Stumpo et al., 2020). Indeed, the increase of the persistent nature of the SYM-H index during the occurrence of storms and substorms could be due to both the external interplanetary medium driver and the internal driving effect on the ring current by high-latitude phenomena (Daglis et al., 1996; De Michelis et al., 2011). Moreover, the increase of its multifractal nature can be read as an indication of the occurrence of intermittent bursts. These bursts can be related both to the occurrence of spatio-temporal turbulence in the equatorial plasma sheet regions and to the impulsive energy-release phenomena. These last phenomena, associated with the AE index burst activity, can also contribute to the information flow towards the magnetospheric equatorial currents (Stumpo et al., 2020). On the other hand, the quasi-invariant nature of the AE index during quiet and disturbed periods seems to support this scenario, posing a serious concern on the key role of high-latitude processes, directly connected with tail current phenomena and dynamics, for correctly characterizing the near-Earth electromagnetic environment dynamics. The auroral activity is indeed representative of both plasma convection inside the magnetosphere and transient activity occurring in the tail region (Lui, Liou, Newell, Meng, Ohtani, Ogino, Kokubun, Brittnacher and Parks, 1998; Sharma, Nakamura, Runov, Grigorenko, Hasegawa, Hoshino, Louarn, Owen, Petrukovich, Sauvaud, Semenov, Sergeev, Slavin, Ã-. Sonnerup, Zelenyi, Fruit, Haaland, Malova and Snekvik, 2008). The former being a large-scale phenomenon related to Southward interplanetary magnetic field conditions, the latter being characterized by a turbulent dynamics in terms of auroral blobs and bursty-bulk-flows (Borovsky, Elphic, Funsten and Thomsen, 1997), also affecting the magnetosphere-ionosphere

system at meso- and small-scale (Lyons, Nishimura and Zou, 2016; Gabrielse, Pinto, Nishimura, Lyons, Gallardo-Lacourt and Deng, 2019). This can be seen as a reflection of a more "dynamic" nature of the AE index, i.e., of the auroral electrojets, mostly sensitive to different kind of processes occurring at different timescales and locations in the magnetosphere-ionosphere system, with respect to a more "global" character of the SYM-H index, whose variability is mostly related to processes occurring on timescales >200 min such as the enhanced convection and the ring-current intensity increases. Thus, monitoring the high-latitude dynamics at high-resolution (at least 1 minute or less) can help in the characterization of several kinds of source mechanisms, which are responsible for many Space Weather phenomena, such as the generation of ground-induced currents due to the fast variability and large enhancements in magnetospheric and ionospheric current systems during major geomagnetic storms (Tozzi, Coco, De Michelis and Giannattasio, 2019a; Tozzi, De Michelis, Coco and Giannattasio, 2019b).

Acknowledgements

The OMNI data were obtained from the Space Physics Data Facility (SPDF) Coordinated Data Analysis Web (CDAWeb) interface at https://cdaweb.gsfc.nasa.gov/index.html/. The authors also acknowledge World Data Center for Geomagnetism (Kyoto) for the use of the geomagnetic indices data. T.A. acknowledges the Institute for Space Astrophysics and Planetology (IAPS) for its support within the framework "Bando Nuove Idee IAPS 2019". G.C and P.D.M. acknowledge financial support by the Italian MIUR-PRIN grant 2017APKP7T on Circumterrestrial Environment: Impact of Sun-Earth Interaction. T.A. and G.C. acknowledge fruitful discussions within the scope of the International Team “Complex Systems Perspectives Pertaining to the Research of the Near-Earth Electromagnetic Environment” at the International Space Science Institute in Bern, Switzerland.

References

Ahn, B.H., Akasofu, S.I., Kamide, Y., 1983. The Joule heat production rate and the particle energy injection rate as a function of the geomagnetic indices AE and AL. Journal of Geophysical Research 88, 6275–6288. doi:10.1029/JA088iA08p06275.

Alberti, T., Consolini, G., Carbone, V., 2019a. A discrete dynamical system: The poor man’s magnetohydrodynamic (PMMHD) equations. Chaos 29, 103107. doi:10.1063/1.5109534.

Alberti, T., Consolini, G., Carbone, V., Yordanova, E., Marcucci, M.F., De Michelis, P., 2019b. Multifractal and Chaotic Properties of Solar Wind at MHD and Kinetic Domains: An Empirical Mode Decomposition Approach. Entropy 21, 320. doi:10.3390/e21030320.

Alberti, T., Consolini, G., De Michelis, P., Laurenza, M., Marcucci, M.F., 2018. On fast and slow Earth’s magnetospheric dynamics during geomagnetic storms: a stochastic Langevin approach. Journal of Space Weather and Space Climate 8, A56. doi:10.1051/swsc/2018039.

Alberti, T., Consolini, G., Lepreti, F., Laurenza, M., Vecchio, A., Carbone, V., 2017a. Timescale separation in the solar wind-magnetosphere coupling during St. Patrick’s Day storms in 2013 and 2015. Journal of Geophysical Research (Space Physics) 122, 4266–4283. doi:10.1002/2016JA023175.

Alberti, T., Laurenza, M., Cliver, E.W., 2019c. Forecasting solar proton events by using the ESPERTA model. Nuovo Cimento C 42, 40. doi:10.1393/ncc/i2019-19040-y.

Alberti, T., Laurenza, M., Cliver, E.W., Storini, M., Consolini, G., Lepreti, F., 2017b. Solar Activity from 2006 to 2014 and Short-term Forecasts of Solar Proton Events Using the ESPERTA Model. The Astrophysical Journal 838, 59. doi:10.3847/1538-4357/aa5cb8.

Alberti, T., Lekscha, J., Consolini, G., De Michelis, P., Donner, R.V., 2020. Disentangling nonlinear geomagnetic variability during magnetic storms and quiescence by timescale dependent recurrence properties. Journal of Space Weather and Space Climate 10, 25. doi:10.1051/swsc/2020026.

Balasis, G., Daglis, I.A., Kapiris, P., Mandea, M., Vassiliadis, D., Eftaxias, K., 2006. From pre-storm activity to magnetic storms: a transition described in terms of fractal dynamics. Annales Geophysicae 24, 3557–3567. doi:10.5194/angeo-24-3557-2006.

Balasis, G., Daglis, I.A., Papadimitriou, C., Kalimeri, M., Anastasiadis, A., Eftaxias, K., 2008. Dynamical complexity in D_{st} time series using non-extensive Tsallis entropy. Geophys. Res. Lett. 35, L14102. doi:10.1029/2008GL034743.

Balasis, G., Daglis, I.A., Papadimitriou, C., Kalimeri, M., Anastasiadis, A., Eftaxias, K., 2009. Investigating dynamical complexity in the magnetosphere using various entropy measures. Journal of Geophysical Research (Space Physics) 114, A00D06. doi:10.1029/2008JA014035.

Balasis, G., Daglis, I.A., Zesta, E., Papadimitriou, C., Georgiou, M., Haagmans, R., Tsinganos, K., 2012. ULF wave activity during the 2003 Halloween superstorm: multipoint observations from CHAMP, Cluster and Geotail missions. Annales Geophysicae 30, 1751–1768. doi:10.5194/angeo-30-1751-2012.

Borovsky, J.E., Elphic, R.C., Funsten, H.O., Thomsen, M.F., 1997. The Earth’s plasma sheet as a laboratory for flow turbulence in high-[beta] MHD. Journal of Plasma Physics 57, 1–34. doi:10.1017/S0022377896005259.

Borovsky, J.E., Osmane, A., 2019. Compacting the description of a time-dependent multivariable system and its multivariable driver by reducing the state vectors to aggregate scalars: the earth’s solar-wind-driven magnetosphere. Nonlinear Processes in Geophysics 26, 429–443. URL: https://www.nonlin-processes-geophys.net/26/429/2019/, doi:10.5194/npg-26-429-2019.

Borovsky, J.E., Valdivia, J.A., 2018. The Earth’s Magnetosphere: A Systems Science Overview and Assessment. Surveys in Geophysics 39, 817–859. doi:10.1007/s10712-018-9487-x.

Bruno, R., Carbone, V., 2016. Turbulence in the Solar Wind. volume 928. doi:10.1007/978-3-319-43440-7.

Carlyle, J., van Driel-Gesztelyi, L., Zuccarello, F., James, A., Williams, D., 2017. The 2015 St Patrick's Day Storm: Origins, in: AAS/Solar Physics Division Abstracts #48, p. 404.02.

Chang, T.T.S., Tam, S.W.Y., Wu, C.C., Consolini, G., 2003. Complexity, Forced and/or Self-Organized Criticality, and Topological Phase Transitions in Space Plasmas. Space Science Reviews 107, 425–445. doi:10.1023/A:1025502023494.

Chi, P.J., Russell, C.T., Foster, J.C., Moldwin, M.B., Engebretson, M.J., Mann, I.R., 2005. Density enhancement in plasmasphere-ionosphere plasma during the 2003 Halloween Superstorm: Observations along the 330th magnetic meridian in North America. Geophys. Res. Lett. 32, L03S07. doi:10.1029/2004GL021722.

Clette, F., Svalgaard, L., Vaquero, J.M., Cliver, E.W., 2014. Revisiting the Sunspot Number. A 400-Year Perspective on the Solar Cycle. Space Science Reviews 186, 35–103. doi:10.1007/s11214-014-0074-2, arXiv:1407.3231.

Consolini, G., 2002. Self-organized criticality: A new paradigm for the magnetotail dynamics. Fractals 10, 275–283. doi:10.1142/S0218348X02001397.

Consolini, G., Alberti, T., De Michelis, P., 2018. On the Forecast Horizon of Magnetospheric Dynamics: A Scale-to-Scale Approach. Journal of Geophysical Research (Space Physics) 123, 9065–9077. doi:10.1029/2018JA025952.

Consolini, G., Chang, T.S., 2001. Magnetic Field Topology and Criticality in Geotail Dynamics: Relevance to Substorm Phenomena. Space Sci. Rev. 95, 309–321.

Consolini, G., De Michelis, P., 1998. Non-Gaussian distribution function of AE-index fluctuations: Evidence for time intermittency. Geophys. Res. Lett. 25, 4087–4090. doi:10.1029/1998GL900073.

Consolini, G., De Michelis, P., 2005. Local intermittency measure analysis of AE index: The directly driven and unloading component. Geophysical Research Letters 32, L05101. doi:10.1029/2004GL022063.

Consolini, G., Marcucci, M.F., Candidi, M., 1996. Multifractal structure of auroral electrojet index data. Phys. Rev. Lett. 76, 4082–4085. URL: https://link.aps.org/doi/10.1103/PhysRevLett.76.4082, doi:10.1103/PhysRevLett.76.4082.

Daglis, I.A., Axford, W.I., Livi, S., Wilken, B., Grande, M., Søraas, F., 1996. Auroral Ionospheric Ion Feeding of the Inner Plasma Sheet during Substorms. Journal of Geomagnetism and Geoelectricity 48, 729–739. doi:10.5636/jgg.48.729.

Daglis, I.A., Livi, S., Sarris, E.T., Wilken, B., 1994. Energy density of ionospheric and solar wind origin ions in the near-Earth magnetotail during substorms. Journal of Geophysical Research 99, 5691–5704. doi:10.1029/93JA02772.

Davis, T.N., Sugiura, M., 1966. Auroral electrojet activity index ae and its universal time variations. Journal of Geophysical Research (1896-1977) 71, 785–801. URL: https://agupubs.onlinelibrary.wiley.com/doi/abs/10.1029/JZ071i003p00785, doi:10.1029/JZ071i003p00785, arXiv:https://agupubs.onlinelibrary.wiley.com/doi/pdf/10.1029/JZ071i003p00785.

De Michelis, P., Consolini, G., Materassi, M., Tozzi, R., 2011. An information theory approach to the storm-substorm relationship. Journal of Geophysical Research (Space Physics) 116, A08225. doi:10.1029/2011JA016535.

Flandrin, P., Rilling, G., Goncalves, P., 2004. Empirical Mode Decomposition as a Filter Bank. IEEE Signal Processing Letters 11, 112–114. doi:10.1109/LSP.2003.821662.

Gabrielse, C., Pinto, V., Nishimura, Y., Lyons, L., Gallardo-Lacourt, B., Deng, Y., 2019. Storm Time Mesoscale Plasma Flows in the Nightside High-Latitude Ionosphere: A Statistical Survey of Characteristics. Geophys. Res. Lett. 46, 4079–4088. doi:10.1029/2018GL081539.

Gonzalez, W.D., Joselyn, J.A., Kamide, Y., Kroehl, H.W., Rostoker, G., Tsurutani, B.T., Vasyliunas, V.M., 1994. What is a geomagnetic storm? J. Geophys. Res. 99, 5771–5792. doi:10.1029/93JA02867.

Gopalswamy, N., Akiyama, S., Yashiro, S., Xie, H., Mäkelä, P., Michalek, G., 2014. Anomalous expansion of coronal mass ejections during solar cycle 24 and its space weather implications. Geophysical Research Letters 41, 2673–2680. doi:10.1002/2014GL059858, arXiv:1404.0252.

Gopalswamy, N., Mäkelä, P., Yashiro, S., Xie, H., Akiyama, S., Thakur, N., 2015. High-energy solar particle events in cycle 24, in: Journal of Physics Conference Series, p. 012012. doi:10.1088/1742-6596/642/1/012012, arXiv:1507.06162.

Harold, E.H., 1951. Long-term storage capacity of reservoirs. Transactions of the American Society of Civil Engineers 116, 2247.

Hathaway, D.H., 2015. The Solar Cycle. Living Reviews in Solar Physics 12, 4. doi:10.1007/lrsp-2015-4, arXiv:1502.07020.

Hausdorff, F., 1918. Dimension und äußeres maß. Mathematische Annalen 79, 157–179. URL: http://www.springerlink.com/content/j3x1t373233w4713.

Huang, N.E., Shen, Z., Long, S.R., Wu, M.C., Shih, H.H., Zheng, Q., Yen, N.C., Tung, C.C., Liu, H.H., 1998. The empirical mode decomposition and the Hilbert spectrum for nonlinear and non-stationary time series analysis. Proceedings of the Royal Society of London Series A 454, 903–998. doi:10.1098/rspa.1998.0193.

Huang, N.E., Wu, Z., 2008. A review on Hilbert-Huang transform: Method and its applications to geophysical studies. Reviews of Geophysics 46, RG2006. doi:10.1029/2007RG000228.

Iyemori, T., 1990. Storm-time magnetospheric currents inferred from mid-latitude geomagnetic field variations. Journal of Geomagnetism and Geoelectricity 42, 1249–1265. doi:10.5636/jgg.42.1249.

Kamide, Y., 1990. The importance of the variability of the solar-terrestrial environment. Washington DC American Geophysical Union Geophysical Monograph Series 60, 23–23. doi:10.1029/GM060p0023.

Kamide, Y., Kokubun, S., 1996. Two-component auroral electrojet: Importance for substorm studies. Journal of Geophysical Research 101, 13027–13046. doi:10.1029/96JA00142.

Kamide, Y., Kusano, K., 2015. No major solar flares but the largest geomagnetic storm in the present solar cycle. Space Weather 13, 365–367. URL: https://agupubs.onlinelibrary.wiley.com/doi/abs/10.1002/2015SW001213, doi:10.1002/2015SW001213, arXiv:https://agupubs.onlinelibrary.wiley.com/doi/pdf/10.1002/2015SW001213.

Klimas, A.J., Vassiliadis, D., Baker, D.N., Roberts, D.A., 1996. The organized nonlinear dynamics of the magnetosphere. Journal of Geophysical Research 101, 13089–13114. doi:10.1029/96JA00563.

Laurenza, M., Alberti, T., Cliver, E.W., 2018. A Short-term ESPERTA-based Forecast Tool for Moderate-to-extreme Solar Proton Events. The Astrophys. J. 857, 107. doi:10.3847/1538-4357/aab712.

Laurenza, M., Alberti, T., Marcucci, M.F., Consolini, G., Jacquey, C., Molendi, S., Macculi, C., Lotti, S., 2019. Estimation of the particle radiation

environment at the l1 point and in near-earth space. The Astrophysical Journal 873, 112. URL: https://doi.org/10.3847%2F1538-4357%2Fab0410, doi:10.3847/1538-4357/ab0410.

Lui, A.T.Y., Liou, K., Newell, P.T., Meng, C.I., Ohtani, S.I., Ogino, T., Kokubun, S., Brittnacher, M.J., Parks, G.K., 1998. Plasma and magnetic flux transport associated with auroral breakups. Geophysical Research Letters 25, 4059–4062. doi:10.1029/1998GL900022.

Lyon, J.G., 2000. The Solar Wind-Magnetosphere-Ionosphere System. Science 288, 1987–1991. doi:10.1126/science.288.5473.1987.

Lyons, L.R., Nishimura, Y., Zou, Y., 2016. Unsolved problems: Mesoscale polar cap flow channels' structure, propagation, and effects on space weather disturbances. Journal of Geophysical Research (Space Physics) 121, 3347–3352. doi:10.1002/2016JA022437.

Mandelbrot, B.B., 1982. The Fractal Geometry of Nature.

Ott, E., 2002. Chaos in Dynamical Systems - 2nd Edition. doi:10.2277/0521811961.

Richardson, I.G., Cane, H.V., 2012. Solar wind drivers of geomagnetic storms during more than four solar cycles. Journal of Space Weather and Space Climate 2, A01. doi:10.1051/swsc/2012001.

Selvakumaran, R., Veenadhari, B., Akiyama, S., Pandya, M., Gopalswamy, N., Yashiro, S., Kumar, S., Mäkelä, P., Xie, H., 2016. On the reduced geoeffectiveness of solar cycle 24: A moderate storm perspective. Journal of Geophysical Research: Space Physics 121, 8188–8202. URL: https://agupubs.onlinelibrary.wiley.com/doi/abs/10.1002/2016JA022885, doi:10.1002/2016JA022885, arXiv:https://agupubs.onlinelibrary.wiley.com/doi/pdf/10.1002/2016JA022885.

Sharma, A.S., 1995. Assessing the magnetosphere's nonlinear behavior: Its dimension is low, its predictability, high. Reviews of Geophysics 33, 645–650. doi:10.1029/95RG00495.

Sharma, A.S., Nakamura, R., Runov, A., Grigorenko, E.E., Hasegawa, H., Hoshino, M., Louarn, P., Owen, C.J., Petrukovich, A., Sauvaud, J.A., Semenov, V.S., Sergeev, V.A., Slavin, J.A., Ã-. Sonnerup, B.U., Zelenyi, L.M., Fruit, G., Haaland, S., Malova, H., Snekvik, K., 2008. Transient and localized processes in the magnetotail: a review. Annales Geophysicae 26, 955–1006. doi:10.5194/angeo-26-955-2008.

Stumpo, M., Consolini, G., Alberti, T., Quattrociocchi, V., 2020. Measuring information coupling between the solar wind and the magnetosphere–ionosphere system. Entropy 22, 276. URL: http://dx.doi.org/10.3390/e22030276, doi:10.3390/e22030276.

Subramanian, S.P., Shanmugaraju, A., 2016. Study of intensive solar flares in the rise phase of solar cycle 23 and 24 and other activities. Astrophysics and Space Science 361, 78. doi:10.1007/s10509-016-2664-9.

Takalo, J., Lohikoski, R., Timonen, J., 1995. Structure function as a tool in AE and Dst time series analysis. Geophysical Research Letters 22, 635–638. doi:10.1029/95GL00053.

Tozzi, R., Coco, I., De Michelis, P., Giannattasio, F., 2019a. Latitudinal dependence of geomagnetically induced currents during geomagnetic storms. Annals of Geophysics 62. doi:10.4401/ag-7788.

Tozzi, R., De Michelis, P., Coco, I., Giannattasio, F., 2019b. A Preliminary Risk Assessment of Geomagnetically Induced Currents over the Italian Territory. Space Weather 17, 46–58. doi:10.1029/2018SW002065.

Tsurutani, B.T., Echer, E., Gonzalez, W.D., 2011. The solar and interplanetary causes of the recent minimum in geomagnetic activity (MGA23): a combination of midlatitude small coronal holes, low IMF B_Z variances, low solar wind speeds and low solar magnetic fields. Annales Geophysicae 29, 839–849. doi:10.5194/angeo-29-839-2011.

Tsurutani, B.T., Judge, D.L., Guarnieri, F.L., Gangopadhyay, P., Jones, A.R., Nuttall, J., Zambon, G.A., Didkovsky, L., Mannucci, A.J., Iijima, B., Meier, R.R., Immel, T.J., Woods, T.N., Prasad, S., Floyd, L., Huba, J., Solomon, S.C., Straus, P., Viereck, R., 2005. The october 28, 2003 extreme euv solar flare and resultant extreme ionospheric effects: Comparison to other halloween events and the bastille day event. Geophysical Research Letters 32. URL: https://agupubs.onlinelibrary.wiley.com/doi/abs/10.1029/2004GL021475, doi:10.1029/2004GL021475, arXiv:https://agupubs.onlinelibrary.wiley.com/doi/pdf/10.1029/2004GL021475.

Tsurutani, B.T., Sugiura, M., Iyemori, T., Goldstein, B.E., Gonzalez, W.D., Akasofu, S.I., Smith, E.J., 1990. The nonlinear response of ae to the imf bs driver: A spectral break at 5 hours. Geophysical Research Letters 17, 279–282. URL: https://agupubs.onlinelibrary.wiley.com/doi/abs/10.1029/GL017i003p00279, doi:10.1029/GL017i003p00279, arXiv:https://agupubs.onlinelibrary.wiley.com/doi/pdf/10.1029/GL017i003p00279.

Uritsky, V.M., Klimas, A.J., Vassiliadis, D., 2002. Multiscale dynamics and robust critical scaling in a continuum current sheet model. Phys. Rev. E 65, 046113. doi:10.1103/PhysRevE.65.046113.

Uritsky, V.M., Pudovkin, M.I., 1998. Low frequency 1/f-like fluctuations of the AE-index as a possible manifestation of self-organized criticality in the magnetosphere. Annales Geophysicae 16, 1580–1588. doi:10.1007/s00585-998-1580-x.

Vainio, R., Raukunen, O., Tylka, A.J., Dietrich, W.F., Afanasiev, A., 2017. Why is solar cycle 24 an inefficient producer of high-energy particle events? Astronomy & Astrophysics 604, A47. doi:10.1051/0004-6361/201730547, arXiv:1707.00485.

Vassiliadis, D., 2006. Systems theory for geospace plasma dynamics. Reviews of Geophysics 44, RG2002. doi:10.1029/2004RG000161.

Verbanac, G., Vršnak, B., Živković, S., Hojsak, T., Veronig, A.M., Temmer, M., 2011. Solar wind high-speed streams and related geomagnetic activity in the declining phase of solar cycle 23. Astrophysics and Space Science 533, A49. doi:10.1051/0004-6361/201116615.

Wanliss, J., 2005. Fractal properties of SYM-H during quiet and active times. Journal of Geophysical Research (Space Physics) 110, A03202. doi:10.1029/2004JA010544.

Wanliss, J., Uritsky, V.M., 2010. Understanding bursty behavior in midlatitude geomagnetic activity. Journal of Geophysical Research (Space Physics) 115, A03215. doi:10.1029/2009JA014642.

Welter, G.S., Esquef, P.A.A., 2013. Multifractal analysis based on amplitude extrema of intrinsic mode functions. Phys. Rev. E 87, 032916. URL: https://link.aps.org/doi/10.1103/PhysRevE.87.032916, doi:10.1103/PhysRevE.87.032916.

Wu, C.C., Liou, K., Lepping, R.P., Hutting, L., Plunkett, S., Howard, R.A., Socker, D., 2016. The first super geomagnetic storm of solar cycle 24: "The St. Patrick's day event (17 March 2015)". Earth, Planets, and Space 68, 151. doi:10.1186/s40623-016-0525-y.